Graphene Oxide/Cellulose Composite for Enhanced Adsorption of Ce(III) from Aqueous Solution

Yan Hao,[a,*] Jing Qu,[a] Zunyi Liu,[a] Hui Yang,[a] Huazheng Sai,[a] Huimin Yang,[a] Jing Peng,[b] Long Zhao,[c] and Maolin Zhai [b,*]

A high-efficiency composite adsorbent was synthesized by mixing cellulose and graphene oxide (GO) in the lithium chloride/N,N-dimethyl-acetamide system. The cellulose/GO composite (D-RCGO) was characterized by scanning electron microscopy, Fourier transform infrared spectroscopy, elemental analysis, and thermal gravimetric analysis. The influences of various parameters on the removal of Ce(III), such as the adsorbent dosage, temperature, initial Ce(III) concentration, contact time, and pH, were optimized using a range of batch adsorption experiments. Adsorption kinetics displayed adsorption behavior according to the Langmuir isotherm model and pseudo-second-order model. The X-ray photoelectron spectroscopy analysis showed that the two peaks of Ce-3d almost disappeared after the desorption in NaCl solution, which indicated that the adsorption belonged to the ion exchange adsorption mechanism. Furthermore, the theoretical maximum capacity of the adsorption of Ce(III) onto D-RCGO was 225.8 $mg \cdot g^{-1}$. This work suggested that the D-RCGO composite membranes could serve as an effective and eco-friendly adsorbent for rare earth pollutant removal in wastewater treatment.

DOI: 10.15376/biores.17.3.4905-4920

Keywords: Graphene oxide; Cellulose; Composite; LiCl/ N,N-dimethylacetamide; Adsorption; Ce(III) ions

Contact information: a: Institute of Applied Chemistry School of Chemistry and Chemical Engineering, Inner Mongolia University of Science & Technology, NO.7 Arden Street, Baotou 014010, P. R. China; b: Radiochemistry and Radiation Chemistry Key Laboratory of Fundamental Science, the Key Laboratory of Polymer Chemistry and Physics of the Ministry of Education, College of Chemistry and Molecular Engineering, Beijing National Laboratory for Molecular Sciences, Peking University, Beijing 100871, P. R. China; c: Institute of Applied Electromagnetic Engineering, Huazhong University of Science and Technology, Wuhan 430074, P. R. China;
** Corresponding authors: haoyannk@163.com; mlzhai@pku.edu.cn*

INTRODUCTION

Due to their distinctive physicochemical properties, rare earth elements (REEs) have found applications in many advanced technologies and high-tech industries, including crude oil refining (Reindl *et al.* 2021), electric vehicle batteries (Crawford *et al.* 2021), lighting indicators, turbine electronic equipment, and other equipment essential to energy and defense sectors. As one important rare earth element, cerium has been extensively used in the rare earth magnetic materials industry (Wang *et al.* 2020), nonferrous alloy additives, storage materials (Singh *et al.* 2008), biomedical applications (Pereao *et al.* 2019), metallurgy, and ceramics (Wang *et al.* 2020). In the environment, most REEs are exclusively present in the trivalent state, but Ce may also occur in the tetravalent state (Gogos *et al.* 2020). It was found that soluble Ce(III) was far more toxic than Ce(IV) when an equal total concentration of Ce was evaluated (Dahle and Arai 2014). In recent years,

the utilization of REEs and production of rare earth-containing products have increased greatly. However, it also creates new environmental problems (Jiao *et al.* 2020). For instance, REEs can interfere with plant growth, damage the ecosystem, and even pose a threat to human health (Gwenzi *et al.* 2018). Long-term intake of low doses of REEs will lead to a decrease in intelligence quotient and a significant reduction in the bioelectrical conduction speed of the central nervous system, and it is difficult to be removed from the body through metabolism (Wang *et al.* 2019b). The common methods to remove rare earth pollutants from the environment are: nanofiltration (Lopez *et al.* 2020), membrane filtration (He *et al.* 2019), and electrodialysis (Li *et al.* 2020). Nevertheless, the above methods require high energy consumption at high cost. In contrast, the adsorption approach has many advantages for rare earth pollutant removal, such as high efficiency, environmental friendliness, and low energy consumption (Li *et al.* 2019b). The key to the adsorption method is to design and prepare suitable adsorbents. The adsorbents currently used to treat rare earth pollutants include activated carbon (Burakova *et al.* 2018), activated alumina (He *et al.* 2019), composite silica, and biomass adsorbents (Li *et al.* 2019a). Among them, biomass adsorbents, such as cellulose, are widely used because of their excellent biodegradability, renewability, and low cost. For example, it has been reported that the hydrogel adsorbent based on carboxymethylcellulose (CMC) has excellent reusability, fast adsorption kinetics, and high adsorption capacity for rare-earth metals La(III) and Ce(III) (Zhu *et al.* 2016).

However, native cellulose adsorbents suffer from low adsorption capacity and poor mechanical properties. The poor mechanical property of native cellulose is due to its own structure, while the low adsorption capacity is because native cellulose only possesses hydroxyl groups on its surface. These problems can be effectively overcome by compounding cellulose with other materials, such as graphene oxide (GO), to form composites. The GO has distinctive two-dimensional spatial structure and contains abundant functional groups, such as epoxy, hydroxyl group, and carboxyl group, for binding (Zhang *et al.* 2015). Hence, GO is considered a promising adsorbent for many metal ions, such as U (VI)/Eu (III) (Zhong *et al.* 2020), Cu (II), Zn (II), Cd (II) (Sitko *et al.* 2013), *etc*. However, using GO alone as an adsorbent has many drawbacks, such as high cost, and difficulty molding and recycling, which limit its practical applications (Zhang *et al.* 2015). Moreover, it is hard to separate the highly water dispersible GO adsorbent from the solution after adsorption, and thus the practical application of GO as an adsorbent is seriously restricted (Cheng *et al.* 2015). Therefore, the cellulose/GO composite adsorbents can take advantage of unique properties of both materials while overcoming their drawbacks. Compounding with cellulose will also improve the molding performance of GO, thereby improving the operability of resultant adsorbents. Zhang *et al.* (2015) prepared a GO/cellulose bead composite by sol-gel method, which exhibited excellent efficiency and reusability for dye pollutants removal. In the authors' previous study, a GO/cellulose composite adsorbent was synthesized by solution blending in ionic liquid system (Hao *et al.* 2019). The results showed that the adsorbent had an excellent adsorption capacity for Ce(III). However, ionic liquids (ILs) used in that work have many disadvantages in practical applications, such as high viscosity and high operating cost. Recent studies have shown that the toxicity of many ILs can be similar to those of the industrial solvents they may replace. A growing body of evidence suggests that they can be toxic to aquatic organisms, including bacteria, plants, invertebrates, and fish (Kulacki and Lamberti 2008). Thus, there is a need to develop new methods to prepare the low cost cellulose/GO

composites without using ionic liquids while maintaining the outstanding adsorption capacity of the adsorbent.

Alternatively, the lithium chloride/N,N-dimethylacetamide (LiCl/DMAc) system could be used as an solvent for cellulose dissolution and subsequent composite formation. LiCl/DMAc has great thermal stability. It dissolves cellulose of high molecule weight directly without degradation or forming any intermediate derivatives (Sayyed *et al.* 2019; Wang *et al.* 2019a). According to Wang *et al.* (2016), LiCl/DMAc can dissolve cellulose with high molecular weight at ambient temperature without acid and alkali. As a very potent solvent of cellulose, LiCl/DMAc can be recycled with a high recovery rate, which accounts for its eco-friendliness. Herein, GO/cellulose composite adsorbents were prepared using LiCl/DMAc as the dissolution solvent in this work. The adsorption performance and mechanism of the adsorbents for Ce(III) were studied systematically. The results demonstrated that the composite could be an excellent adsorbent for REEs in wastewater treatment.

EXPERIMENTAL

Materials

Microcrystalline cellulose (MCC) was supplied by Tianjin Guangfu Fine Chemical Research Institute. The GO was obtained from Changzhou Sixth Element Materials Technology Research Institute (Changzhou, China). N,N-Dimethylacetamide (DMAc) and $LiCl·H_2O$ were purchased from Zhiyuan Chemical Reagent Research Institute (Tianjin, China) and Chemical Plant of Beijing (Beijing, China), respectively. $Ce(NO_3)_3·6H_2O$ was purchased from Damao Chemical Reagent Factory (Tianjin, China). Arsenazo III was purchased from Chemical plant of Beijing Chemical Industry Research Institute (Beijing, China).

Pretreatment of Cellulose

$LiCl·H_2O$ was dried in a vacuum oven before use. A total of 8.40 g of dried LiCl and 84.96 g of DMAc were added into a 100 mL Erlenmeyer flask. The LiCl/DMAc (91/9, w/w) solution was obtained after the ultrasonic treatment (100 W, 30 °C) for 1 h.

The MCC and LiCl/DMAc solvent were added into a three-neck round-bottom flask and mechanically stirred and heated at 160 ℃ for 30 min to make 5 wt% MCC solution. Then, the temperature was raised to 180 °C for 2 min. Subsequently, the pretreated cellulose was filtered out with a sand core funnel and dried under a vacuum at 60 °C for 12 h.

Preparation of Cellulose Colloid

The pretreated cellulose was added into LiCl/DMAc (91/9) solution at 5 wt% and stirred at 90 °C for 3 h to obtain cellulose colloid. A small part of the prepared cellulose colloid was used to make a thin membrane that was washed with deionized water until the silver nitrate test showed no white precipitation. Thereafter, the membrane was further dried in a 60 °C vacuum oven to obtain a regenerated cellulose membrane (D-RC) for comparative experiment.

Preparation of the Composites

A certain amount of GO was dispersed into LiCl/DMAc solution with ultrasonic treatment (60 W, 30 °C) for 1 h, yielding a GO suspension at 0.5 mg·mL^{-1}. The cellulose colloid was mixed with the above GO/ LiCl/DMAc suspension at different mass ratios of 96:4 (named D-RCGO-I) and 98.4:1.6 (named D-RCGO-II). The subsequent cleaning and drying steps were the same as those of D-RC.

Characterization

The micro-Fourier transform infrared (FTIR) spectra of samples in the range of 650 to 4000 cm^{-1} were measured using a spotlight-200 Fourier transform infrared spectroscope (Perkin Elmer company, Waltham, America). The detector is mercury cadmium telluride (MCT), and the beam-splitter is KBr/Ge. The samples were flattened by diamond plates and then analyzed. Micro-FTIR analysis was performed in reflected mode. Thermal gravimetric analysis (TGA) was performed using a Q50 thermal analyzer (TA Instruments company, New Castle, America) at a heating rate of 10 °C·min^{-1} from room temperature to 600 °C in nitrogen atmosphere. The thermal degradation temperature (T_{onset}) was the peak temperature value in the derivative thermogravimetry (DTG) curve. A scanning electron microscope (SEM) (Hitachi S-4800, Hitachi Limited, Tokyo, Japan) was used to characterize the microstructure of the samples before and after compounding. All samples were sputter coated with gold (JFC-1600, Japan Electronics Co., Ltd, Tokyo, Japan) before the test. The ultraviolet- visible (UV-vis) analysis was performed using an ultraviolet visible spectrophotometer (Cintra1010, GBC Scientific Equipment Ltd., Melbourne, Australia). Elemental analyses (EA) were conducted on a MICRO-CUBE element analyzer (Elementar Analysensysteme GmbH, Hanau, Germany) to analyze the percentage of elements of samples. The surface area and pore size distributions of the samples were determined by N_2 adsorption-desorption measurements using the Brunauer–Emmett–Teller (BET, ASAP2460, Micromeritics Instrument Co., Georgia, America). Before the test, the samples were degassed at 60 °C in a vacuum oven for 12 h. After degassing, the nitrogen adsorption/desorption isotherms test was carried out automatically according to the procedure at 77 K. X-ray photoelectron spectroscopy (XPS) analysis (AXIS-Ultra, Kratos Analytical Company, Manchester, Britain) was used to analyze the surface chemical composition of the samples. The excitation source was Al Kα X-ray. The power was 225 W; the current was15 mA; the voltage was 15 kV; and the vacuum degree was 3×10^{-9} mbar. In addition, C1's peak of hydrocarbons was used to calibrate the electron binding energy (BE, 284.8 eV).

Batch Adsorption of Ce(III)

Kinetic study

In a typical procedure, as-synthesized adsorbents (5 mg) were added into the stock solution of Ce(III) (20 mL, 126 mg·L^{-1}, pH=3.1). Afterwards, the system was placed in an incubator at 25 °C and taken out at different time intervals for concentration measurement. The concentration of Ce(III) in the solution was determined by Arsenazo III spectrophotometry as follows: 4.5 mL of the solution was aliquoted out and, Arsenazo III aqueous solution (1 mL, 0.1 wt%) was added. The mixture was mixed well and placed at room temperature for 30 min. The concentration of Ce(III) was determined by measuring the characteristic absorbance at 655 nm with a UV-Vis spectrophotometer. The adsorption capacity of the adsorbent was calculated according to Eqs 1.

$$q = \frac{(C_0 - C) \times V}{m} \quad (1)$$

where C_0 is the initial concentration (mg·L^{-1}) of Ce(III), C is the concentration (mg·L^{-1}) of Ce(III) after adsorption, V (mL) is the total volume of the solution, and m (mg) is the mass of the adsorbent.

Effects of adsorbent dosage and pH

To study the effects of absorbent dosage on its adsorption capacity, different amounts of absorbent were added into 20 mL stock solutions of Ce(III) and the solutions were kept at 25 °C for 120 min to reach adsorption equilibrium. The solutions were filtered, and the concentrations of Ce(III) were quantified to calculate the adsorption capacities at each absorbent dosage. The influence of pH values in the range of 1 to 10 on its adsorption capacity was also studied using a similar procedure as above. The pH values of each sample were adjusted with either HNO_3 (0.1 mol·L^{-1}) or NaOH (0.1 mol·L^{-1}) using pH meter (PHS-3E).

Desorption of D-RCGO-I

After reaching adsorption equilibrium in Ce(III) solution, the D-RCGO-I adsorbent was removed and soaked in NaCl solution (1 mol·L^{-1}) for 12 h and washed with deionized water three times. Then, the samples were dried in a vacuum oven at 60 °C for 24 h and then analyzed by XPS.

Regeneration and reusability of D-RCGO-I

Regeneration and reusability are two important metrics to evaluate the performance of adsorbents. Accordingly, the adsorbent D-RCGO-I that had reached the adsorption equilibrium in Ce(III) solution was taken out and then immersed in HCl (2 mol·L^{-1}) for 24 h at room temperature. The adsorbent was washed with deionized water three times, and dried in a vacuum oven at 60 °C for 24 h. Subsequently, the regenerated absorbent was used to adsorb Ce(III) again and adsorption capacity was measured. The above process was done four times to study the reusability of the adsorbent.

RESULTS AND DISCUSSION

Characterization of D-RCGO

The elemental contents of in GO, D-RCGO-I, and D-RC were determined by elemental analysis, and the results are shown in Table 1. The content of N in D-RCGO-I and D-RC was close to 0, indicating that DMAc was removed from both adsorbents. Furthermore, the silver nitrate test indicated that LiCl was also thoroughly eliminated. As shown in Fig. 1(a), the FTIR spectrum of GO showed two peaks at 1036 and 1719 cm^{-1}, which were attributed to the C-O-C and C=O stretching vibrations, respectively (He *et al.* 2013). The broad peak between 3000 to 3700 cm^{-1} was due to the stretching vibration of -OH, while the peak at 1613 cm^{-1} represented the C=C stretching vibration of GO (Saleh *et al.* 2017). In the spectrum of D-RC shown in Fig. 1(b), the absorption peak at 3343 cm^{-1} was the stretching vibration of -OH. In the region of 1200 to 1500 cm^{-1}, the bending and rocking vibrations of -CH, CH_2, and -OH were dominant. Among them, the peak at 1371 cm^{-1} corresponded to the bending vibration of -CH, and 1318 cm^{-1} represented the bending

vibration of CH_2. Similar to many polysaccharide compounds, cellulose has the chemical structure of C-O-C-O-C diether, whose vibration appeared at approximately 1162 cm^{-1}. As shown in Fig. 1(c), the FTIR spectrum of D-RCGO-I had characteristic absorption peaks of GO and cellulose. For example, the peaks at 1373 and 2897 cm^{-1} represented the C-H stretching vibration and bending vibration of cellulose six-membered ring. In addition, the absorption peak of C=O bond in D-RCGO-I shifted to a lower wavenumber, which was caused by the formation of hydrogen bond between -COOH in GO and -OH in cellulose (Zhang *et al.* 2015). Moreover, the absence of the absorbance at 1719 cm^{-1} in D-RCGO-I by comparing with that of GO also implied that the hydrogen bond was formed between the carboxyl groups of GO and cellulose (Fan *et al.* 2014). These results indicated that GO and cellulose were successfully compounded in LiCl/DMAc.

Moreover, it is reported that the theoretical content of C element in GO and cellulose was about 45% and 44%, respectively (Song *et al.* 2014). From this, it can be theoretically inferred that the content of C element in D-RCGO-I was about 44%, which was consistent with the experimental results of EA data, as shown in Table 1.

Table 1. Elemental Analysis Data of Samples

Sample	C (%)	H (%)	N (%)
GO	47.2	2.7	0.02
MCC	42.7	6.7	0.02
D-RC	41.9	6.8	0.07
D-RCGO-I	42.6	6.5	0.05

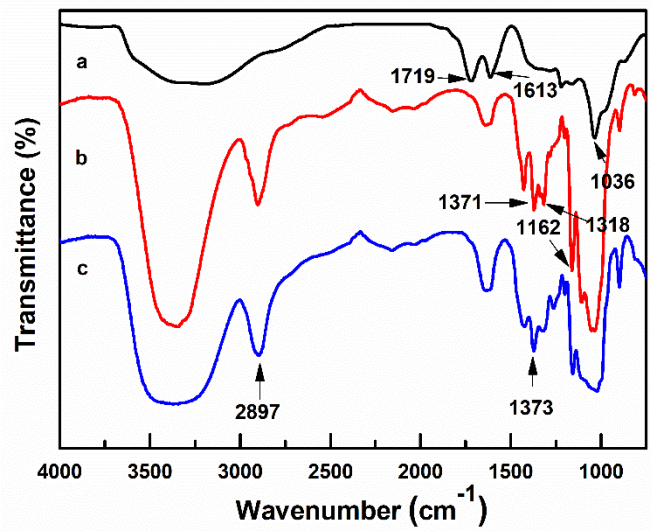

Fig. 1. Micro-FTIR spectra of GO (a), D-RC (b), and D-RCGO-I (c)

According to the TGA results in Fig. 2A, there was a small mass loss in all samples in the temperature range close to 100 °C, due to the evaporation of water. The peak temperature of the DTG curve was defined as T_{max}. As shown in Fig. 2B, T_{max} of GO and MCC were 199 °C and 342 °C, respectively. The mass loss of GO in the temperature range of 120 to 250 °C was about 25.4 wt%, which was attributed to the pyrolysis of unstable oxygen-containing groups in GO (Yuan *et al.* 2014). As shown in Fig. 2A(d), the thermal degradation of MCC started at approximately 300 °C, and gradually reached maximum at T_{max}. Moreover, the char yield was approximately 5 wt% after thermal decomposition at

700 °C. The char yields of D-RC and D-RCGO-I were 12 wt% and 18 wt%, respectively, which were noticeably higher than that of MCC. The main reason was that the thermal degradation of cellulose was caused by depolymerization of cellulose to low molecular weight oligosaccharides. Afterwards, the scission of D-glucopyranosyl group was initiated with the increase of temperature (Lin *et al.* 2009). The char formation was due to the crosslinking and repolymerization of pyrolysis products. During thermal degradation, the amorphous cellulose was degraded first, leading to the high char formation and low degree crystallinity in D-RC and D-RCGO-I (Abbott and Bismarck 2010).

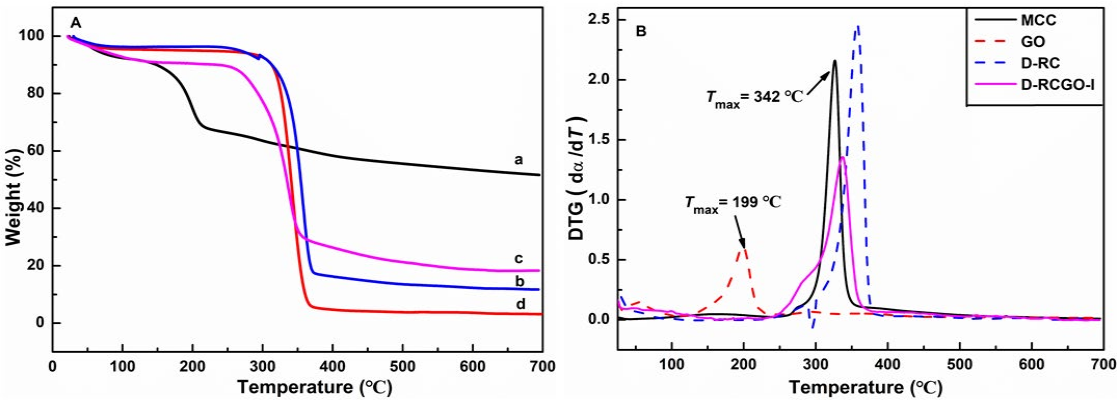

Fig. 2. TGA curves of GO (a), D-RC (b), D-RCGO-I (c), and MCC (d) (A); DTG curves of above samples (B)

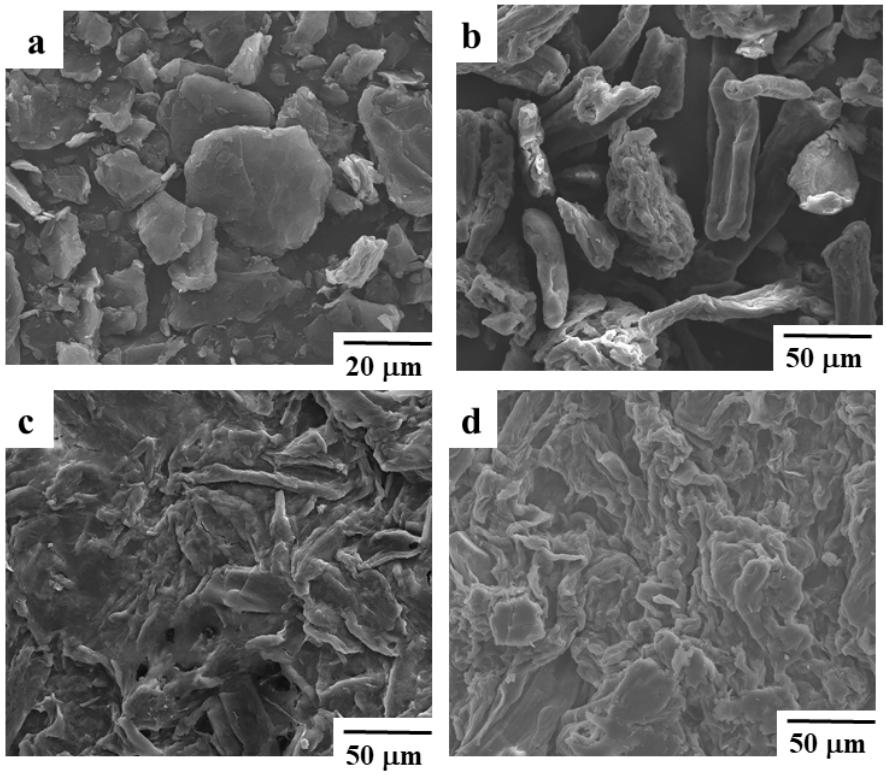

Fig. 3. SEM micrographs of GO (a), MCC (b), D-RC (c), and D-RCGO-I (d)

The morphology of GO, D-RC, and D-RCGO-I was characterized using SEM (Fig. 3). In Fig. 3(a) and (b), the lamellar structure of GO and a strip curl morphology of MCC could be observed. In contrast to original MCC, both D-RC and D-RCGO-I showed uniform a laminated structure after being regenerated from the LiCl/DMAc solution (Mahadeva *et al.* 2013). Compared with the micromorphology of GO/cellulose composite adsorbent prepared in ionic liquids from the authors' previous work (Hao *et al.* 2019), the D-RCGO-I membrane was much looser and rougher, which could make it more conducive to efficient adsorption (Fig. 2(d)). Meanwhile, as shown in Table 2, the average pore size of D-RCGO-I and D-RCGO-II was 11.3 and 20.2 nm, respectively. Moreover, the BET surface area of D-RCGO-I (20.0 $m^2 \cdot g^{-1}$) was larger than that of D-RCGO-II (15.6 $m^2 \cdot g^{-1}$), indicating that D-RCGO-I had the potential to be more conducive to adsorption of Ce(III).

Table 2. The Average Pore Size of Samples

Sample	GO	D-RC	D-RCGO-I	D-RCGO-II
Average pore size (nm)	22.2	32.4	11.3	20.2

Investigation of Adsorption Performance of Adsorbents for Ce(III)

Adsorption kinetics

To ensure that the adsorption reached the adsorption equilibrium, the adsorption kinetics of adsorbents were measured first. As shown in Fig. 4A, at the initial stage of adsorption, the adsorption capacity of adsorbents rapidly increased with the increase of adsorption time, as there were many active binding sites on the surface of adsorbents.

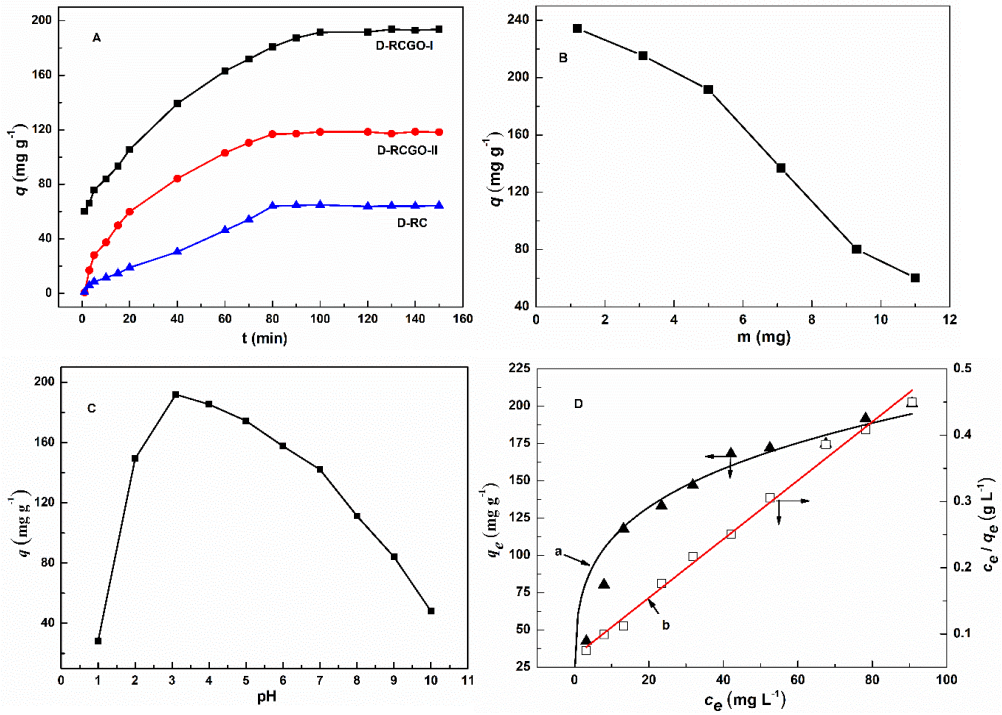

Fig. 4. Kinetics of Ce(III) adsorption onto two different D-RCGO adsorbents and D-RC at room temperature (pH: 3.1; adsorbent dosage: 5 mg) (A); Effect of adsorbent dosage of D-RCGO-I on the uptake of Ce(III) (adsorption time: 120 min; temperature: 25 °C; pH: 3.1) (B); Effect of solution pH on the adsorption of Ce(III) by D-RCGO-I (adsorption time: 120 min; adsorbent dosage: 5 mg) (C); Adsorption isotherm of D-RCGO-I (a) and Langmuir linear plot (b) (adsorption time: 120 min; pH: 3.1; adsorbent dosage: 5 mg) (D)

The adsorption capacity gradually reached the plateau at approximately 100 min when the active sites were gradually occupied by Ce(III) ions. To ensure the adsorption equilibrium, 120 min was hence chosen as the adsorption time in the following adsorption experiments. The order of adsorption capacity at 120 min was D-RCGO-I > D-RCGO-II > D-RC. Therefore, D-RCGO-I was selected in subsequent experiments to systematically study the adsorption performance for Ce(III).

The two kinetic models of pseudo-first-order and pseudo-second-order were used to fit the adsorption kinetic data of D-RCGO-I. As shown in Table 3, the linear coefficient of determination (R^2) using the pseudo-second-order kinetic model was 0.991, which was higher than that of the pseudo-first-order fitting. These results suggested that a diffusion process into a network of small pores controlled the rate of the adsorption of Ce(III) on the adsorbent D-RCGO-I (Hubbe *et al.* 2019).

Table 3. Fitting Results of the Adsorption of Ce(III) onto D-RCGO-I Using Pseudo-first-order and Pseudo-second-order Kinetic Model

Model	q_{exp} ($mg \cdot g^{-1}$)	k	q_e ($mg \cdot g^{-1}$)	R^2
Pseudo-first-order	191.6	1.75	142.86	0.593
Pseudo-second-order	191.6	0.00037	209.21	0.991

Note: q_{exp} is the experimental value when D-RCGO-I was used to adsorb Ce(III)

Effect of adsorbent dosage and solution pH

The effects of adsorbent dosage on adsorbent D-RCGO-I were studied, and results are shown in Fig. 4B. The adsorption capacity of the adsorbent decreased with increasing adsorbent dosage. This can be explained by the fact that with the increasing dosage of the adsorbent, the excess binding sites on the adsorbent led to lower utilization efficiency and hence lower adsorption capacity.

The influence of solution pH on the adsorption capacity is shown in Fig. 4C. In the range of pH 1 to 4, cerium exists mainly in the form of Ce(III) ion. When the pH was less than 2, H^+ in the solution competed with Ce(III) for the active sites on the adsorbent, resulting in the low adsorption capacity. With the increase of pH value, the adsorption capacity also increased. The maximal adsorption capacity for Ce(III) was 191.6 $mg \cdot g^{-1}$ at pH 3.1, indicating that D-RCGO-I exhibited outstanding adsorption performance for Ce(III) under strong acidic condition. When pH exceeded 4, Ce(III) existed mainly as hydrated ions, such as $Ce(OH)^{2+}$, $Ce(OH)_2^+$, and $Ce(OH)_4^-$ (Abellan *et al.* 2017). The adsorption capacity of D-RCGO-I adsorbent for these ions was much lower than that for Ce(III) ion, which led to the decrease of adsorption capacity of the adsorbent for Ce(III). As the pH further increased beyond 8, the adsorption capacity decreased noticeable, mainly due to the formation of $Ce_2(OH)_3$.

Adsorption isotherm

To further study the adsorption mechanism of adsorbent D-RCGO-I for Ce(III), the equilibrium adsorption data were fit to the Langmuir (Fig. 4D) and Freundlich isotherm models. Moreover, the theoretical maximum adsorption capacity (q_m) of adsorbent was calculated by the adsorption models, which could be used to compare adsorption

performances of different adsorbents. The Freundlich isotherm model (Eq. 2) and Langmuir isotherm model (Eq. 3) can be expressed as follows,

$$\ln\frac{q_t}{K_F} = \frac{1}{n}\ln C_t \quad (2)$$

$$C_e(q_m - q_e) = \frac{q_e}{K_L} \quad (3)$$

where K_L (mg·L^{-1}) and K_F (mg·L^{-1}) are the Langmuir constant and Freundlich model constant, respectively; n is the adsorption degree of the adsorbent; C_e (mg·L^{-1}) and q_e (mg·g^{-1}) are the equilibrium concentration of Ce(III) and the adsorption capacity of the corresponding adsorbent in the solution; q_m (mg·g^{-1}) is the maximum adsorption capacity of the adsorbent; and C_e and q_e are the concentration and adsorption capacity at equilibrium in the solution, respectively.

The fitting results of the two isotherm adsorption models are shown in Table 4. Herein, the Langmuir isotherm model assumes that the adsorption process is based on monolayer coverage of equal sites on the surface of adsorbent (Langmuir 1918), while the Freundlich isotherm is suitable for the adsorption that is on a heterogeneous surface (Ng *et al.* 2002). As shown in Table 4, the value of R^2 of the Langmuir isotherm model was 0.992, which was better that that of Freundlich isotherm model. It suggested that Langmuir isotherm model was a better fit for the adsorption process of the adsorbent. According to Eq. 3, the theoretical maximum adsorption capacity of D-RCGO-I was 225.8 mg·g^{-1}, which was higher than other adsorbents reported in the literature (Behdani *et al.* 2013; Chen *et al.* 2015; Torab-Mostaedi *et al.* 2015). Although the theoretical maximum adsorption capacity of D-RCGO-I was lower than that of CMC-*g*-PAA adsorbents reported in the literature (Zhu *et al.* 2016), D-RCGO-I has better environmental friendliness. This was due to the toxic nature of acrylic acid (AA). Exposure to acrylic acid (AA) causes many diseases and is associated with skin allergy, a strong irritant to mucous membrane and eyes, while long-term exposure may affect the lungs and kidneys (Sverdrup *et al.* 2001).

Table 4. Isotherm Constants and Correlation Coefficients for Ce(III) Adsorption onto D-RCGO-I

Model	Langmuir			Freundlich		
	q_m (mg·g^{-1})	K_L (L·mg^{-1})	R^2	K_F (L·g^{-1})	n	R^2
D-RCGO-I	225.8	0.067	0.992	31.62	2.33	0.935

Desorption performance and regeneration of the adsorbent

After reaching equilibrium in Ce(III) solution, the D-RCGO-I adsorbent was placed in NaCl solution (1 mol·L^{-1}) for desorption experiment. As shown in Fig. 5A, the adsorption capacity of D-RCGO-I for Ce(III) sharply decreased with increasing NaCl concentration, which was attributed to the competition between Ce(III) and Na(I) ions for active binding sites on the adsorbent. To further investigate the adsorption mechanism of D-RCGO-I for Ce (III), the adsorbent after adsorption and desorption was characterized by XPS, as shown in Fig. 5B. After the adsorption of Ce(III) onto D-RCGO-I, the characteristic Ce_{3d} peaks appeared at 885.3 and 903.9 eV (Paparazzo 2011). However, a new peak of Na_{1s} appeared at BE of 1071.8 eV and the peaks of Ce_{3d} almost vanished after

the desorption in NaCl solution, indicating that the Ce(III) was replaced by Na(I) during the desorption process. The results suggested that the Ce(III) was adsorbed onto adsorbent D-RCGO-I via the ion exchange adsorption mechanism.

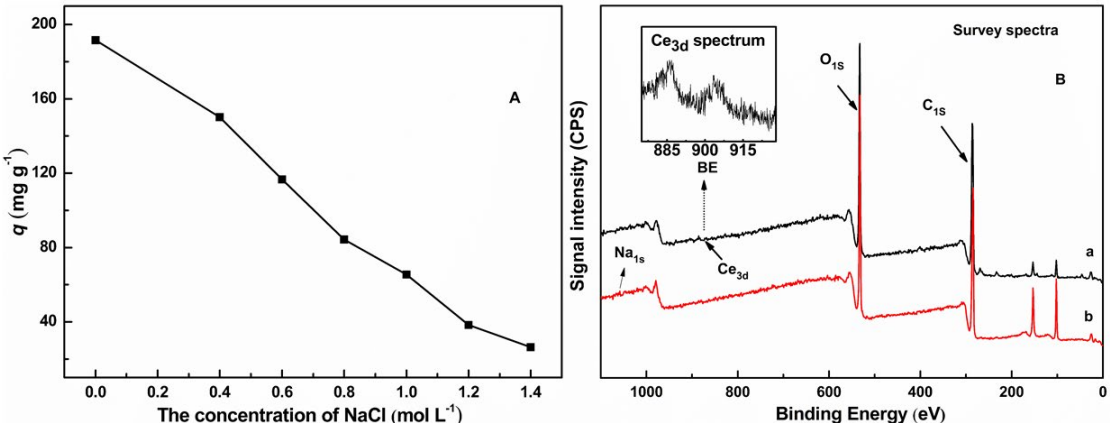

Fig. 5. Effect of NaCl concentration on the adsorption of D-RCGO-I for Ce(III) (temperature: 25 °C; pH: 3.1; adsorption time: 120 min; adsorbent dosage: 5 mg) (A); XPS spectra of D-RCGO-I after adsorption of Ce(III) (a) and D-RCGO-I after desorption using 1 mol·L^{-1} NaCl (b) (B)

As shown in Fig. 6, adsorbent could be recycled by immersing in 2 mol·L^{-1} HCl. The adsorption capacity of the regenerated adsorbent was as high as 172.2 mg·g^{-1}. Although the adsorption capacity decreased to 45.3 mg·g^{-1} after 4 cycles, it was still higher than those of adsorbents reported in many studies (Kütahyali *et al.* 2010; Sert *et al.* 2008). The regeneration rate (r) of adsorbent was calculated using Eq. 4, and presented in Table 5,

$$r = \frac{q_n}{q_0} \tag{4}$$

where q_n (mg·g^{1}) is the adsorption capacity of adsorbent for Ce(III) after regeneration for n times, q_0 (mg·g^{1}) is the adsorption capacity of adsorbent for Ce(III) before regeneration.

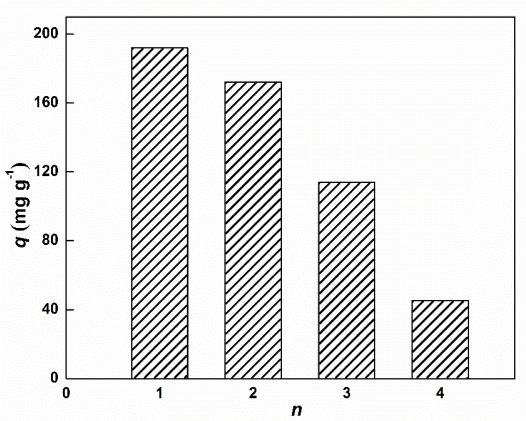

Fig. 6. Effect of regeneration cycles on the adsorption of D-RCGO-I for Ce(III) (temperature: 25 °C; pH: 3.1; adsorption time: 120 min; adsorbent dosage: 5 mg)

Table 5. Adsorption Capacities of Regenerated Adsorbent D-RCGO-I Using HCl as the Regeneration Reagent

Results	Times (*n*) of Regeneration			
	1	2	3	4
q_n ($mg \cdot g^{-1}$)	191.9	172.2	113.9	45.3
Rate of Regeneration (%)	-	89.7	59.4	23.6

CONCLUSIONS

1. The graphene oxide (GO)/cellulose composite adsorbent with high adsorption capacity, fast binding kinetics, and great reusability was successfully prepared by solution blending method using LiCl/DMAc.
2. The adsorption equilibrium could be reached within 100 min and the theoretical maximum adsorption capacity of D-RCGO-I for Ce(III) was 225.8 $mg \cdot g^{-1}$, which is much higher than most of adsorbents reported previously. It was also found out that D-RCGO exhibited outstanding adsorption performance even under the strong acidic condition with the adsorption capacity as high as 191.6 $mg \cdot g^{-1}$ at pH 3.1.
3. The pseudo-second-order adsorption kinetic model was found to fit the adsorption kinetics perfectly. Moreover, XPS analysis suggested that the adsorption mechanism was mainly based on ion exchange.
4. The adsorbent showed reusability, as it could be regenerated using NaCl solution or HCl solution. In summary, D-RCGO prepared in this work demonstrated advantages of high adsorption capacity under high acidity and fast adsorption rate. The resultant D-RCGO could be an excellent adsorbent for the treatment of rare earth ions in wastewater.

ACKNOWLEDGMENTS

This research was funded by National Natural Science Foundation of China (NNSFC, No. 11965015), Program for Young Talents of Science and Technology in Universities of Inner Mongolia Autonomous Region (No. NJYT22072), and the Outstanding Youth Fund Project of Innovation Fund of Inner Mongolia University of Science and Technology (No. 2019YQL05). This work is also supported by the Innovation Fund of Inner Mongolia University of Science & Technology (2018QDL-B01), the Natural Science Foundation of Inner Mongolia (2019BS05022), and the Inner Mongolia Science & Technology Project Plan (NJZZ20087).

REFERENCES CITED

Abbott, A., and Bismarck, A. (2010). "Self-reinforced cellulose nanocomposites," *Cellulose* 17(4), 779-791. DOI: 10.1007/s10570-010-9427-5

Abellan, P., Moser, T., Lucas, I., Grate, J. W., Evans, J., and Browning, N. (2017). "The formation of cerium(III) hydroxide nanoparticles by a radiation mediated increase in local pH," *RSC Advances* 2017(7), 3831-3837. DOI: 10.1039/c6ra27066b

Behdani, F. N., Rafsanjani, A. T., Torab-Mostaedi, M., and Mohammadpour, S. M. A. K. (2013). "Adsorption ability of oxidized multiwalled carbon nanotubes towards aqueous Ce(III) and Sm(III)," *Korean Journal of Chemical Engineering* 30(2), 448-455. DOI: 10.1007/s11814-012-0126-9

Burakova, I. V., Burakov, A. E., Tkachev, A. G., Troshkina, I. D., Veselova, O. A., Babkin, A. V., Wei, M. A., and Ali, I. (2018). "Kinetics of the adsorption of scandium and cerium ions in sulfuric acid solutions on a nanomodified activated carbon," *Journal of Molecular Liquids* 253, 277-283. DOI: 10.1016/j.molliq.2018.01.063

Chen, T., Yan, C., Wang, Y., Tang, C., Zhou, S., Zhao, Y., Ma, R., and Duan, P. (2015). "Synthesis of activated carbon-based amino phosphonic acid chelating resin and its adsorption properties for Ce(III) removal," *Environmental Technology* 36(17), 2168-2176. DOI: 10.1080/09593330.2015.1023365

Cheng, Z., Liao, J., He, B., Zhang, F., Zhang, F., Huang, X., and Zhou, L. (2015). "One-step fabrication of graphene oxide enhanced magnetic composite gel for highly efficient dye adsorption and catalysis," *ACS Sustainable Chemistry & Engineering* 3(7), 1677-1685. DOI: 10.1021/acssuschemeng.5b00383

Crawford, S. E., Ellis, J. E., Ohodnicki, P. R., and Baltrus, J. P. (2021). "Influence of the anionic zinc-adeninate metal-organic framework structure on the luminescent detection of rare earth ions in aqueous streams," *ACS Applied Materials & Interfaces* 13(6), 7268-7277. DOI: 10.1021/acsami.0c20990

Dahle, J. T., and Arai, Y. (2014). "Effects of Ce(III) and CeO_2 nanoparticles on soil-denitrification kinetics," *Archives of Environmental Contamination and Toxicology* 67(4), 474-482. DOI: 10.1007/s00244-014-0031-9

Fan, L., Liu, G., Wu, J., Liu, L., Lin, J., and Wei, Y. (2014). "Asymmetric supercapacitor based on graphene oxide/polypyrrole composite and activated carbon electrodes," *Electrochimica Acta* 137, 26-33. DOI: 10.1016/j.electacta.2014.05.137

Gogos, A., Wielinski, J., Voegelin, A., Kammer, F. v. d., and Kaegi, R. (2020). "Quantification of anthropogenic and geogenic Ce in sewage sludge based on Ce oxidation state and rare earth element patterns," *Water Research X* 9, article ID 100059. DOI: 10.1016/j.wroa.2020.100059

Gwenzi, W., Mangori, L., Danha, C., Chaukura, N., Dunjana, N., and Sanganyado, E. (2018). "Sources, behaviour, and environmental and human health risks of high-technology rare earth elements as emerging contaminants," *Science of The Total Environment* 636, 299-313. DOI: 10.1016/j.scitotenv.2018.04.235

Hao, Y., Cui, Y., Peng, J., Zhao, N., Li, S., and Zhai, M. (2019). "Preparation of graphene oxide/cellulose composites in ionic liquid for Ce(III) removal," *Carbohydrate Polymers* 208, 269-275. DOI: 10.1016/j.carbpol.2018.12.068

He, G., Liu, W., Sun, X., Chen, Q., Wang, X., and Chen, H. (2013). "Fe_3O_4@graphene oxide composite: A magnetically separable and efficient catalyst for the reduction of

nitroarenes," *Materials Research Bulletin* 48(5), 1885-1890. DOI: 10.1016/j.materresbull.2013.01.038

He, Y., Zhang, L., An, X., Wan, G., Zhu, W., and Luo, Y. (2019). "Enhanced fluoride removal from water by rare earth (La and Ce) modified alumina: Adsorption isotherms, kinetics, thermodynamics and mechanism," *Science of The Total Environment* 688, 184-198. DOI: 10.1016/j.scitotenv.2019.06.175

Hubbe, M. A., Azizian, S., and Douven, S. (2019). "Implications of apparent pseudo-second-order adsorption kinetics onto cellulosic materials: A review," *BioResources* 14(3), 7582-7626. DOI: 10.15376/biores.14.3.7582-7626

Jiao, Y., Yang, L., Kong, Z., Shao, L., Wang, G., Xiaofei, R., and Yongjun, L. (2020). "Evaluation of trace metals and rare earth elements in mantis shrimp Oratosquilla oratoria collected from Shandong Province, China, and its potential risks to human health-ScienceDirect," *Marine Pollution Bulletin* 162, article ID 111815. DOI: 10.1016/j.marpolbul.2020.111815

Kulacki, K. J., and Lamberti, G. A. (2008). "Toxicity of imidazolium ionic liquids to freshwater algae," *Green Chemistry* 10(1), 104-110. DOI: 10.1039/b709289J

Kütahyali, C., Sert, Ş., Çetinkaya, B., Inan, S., and Eral, M. (2010). "Factors affecting lanthanum and cerium biosorption on *Pinus brutia* leaf powder," *Separation Science and Technology* 45(10), 1456-1462. DOI: 10.1080/01496391003674266

Langmuir, I. (1918). "The adsorption of gases on plane surfaces of glass, mica and platinum," *Journal of the American Chemical Society* 40(9), 1361-1403. DOI: 10.1021/ja02242a004

Li, C., Ramasamy, D. L., Sillanpää, M., and Repo, E. (2020). "Separation and concentration of rare earth elements from wastewater using electrodialysis technology," *Separation and Purification Technology* 254, article ID 117442. DOI: 10.1016/j.seppur.2020.117442

Li, M., Meng, X., Huang, K., Feng, J., and Jiang, S. (2019a). "A novel composite adsorbent for the separation and recovery of indium from aqueous solutions," *Hydrometallurgy* 186, 73-82. DOI: 10.1016/j.hydromet.2019.04.003

Li, Y., Fan, S., and Zhou, Q. (2019b). "Synthesis of carboxyl-rich biosorbent by UV-induced graft polymerization method for high efficiency adsorption of Ce^{3+} from aqueous solution: Activation and adsorption mechanism," *Journal of Polymers the Environment* 27(10), 2259-2266. DOI: 10.1007/s10924-019-01515-x

Lin, Y., Cho, J., Tompsett, G. A., Westmoreland, P. R., and Huber, G. W. (2009). "Kinetics and mechanism of cellulose pyrolysis," *The Journal of Physical Chemistry C* 113(46), 20097-20107. DOI: 10.1021/jp906702p

Lopez, J., Reig, M., Vecino, X., and Cortina, J. L. (2020). "Arsenic impact on the valorisation schemes of acidic mine waters of the Iberian Pyrite Belt: Integration of selective precipitation and spiral-wound nanofiltration processes," *Journal of Hazardous Materials* 403, article ID 123886. DOI: 10.1016/j.jhazmat.2020.123886

Mahadeva, S. K., Yang, S. Y., and Kim, J. (2013). "Effects of solvent systems on its structure, properties and electromechanical behavior of cellulose electro-active paper," *Current Organic Chemistry* 17(1), 83-88. DOI: 10.2174/138527213805289114

Ng, C., Losso, J. N., Marshall, W. E., and Rao, R. M. (2002). "Freundlich adsorption isotherms of agricultural by-product-based powdered activated carbons in a geosmin-water system," *Bioresource Technology* 85(2), 131-135. DOI: 10.2174/138527213805289114

Paparazzo, E. (2011). "Some notes on XPS Ce_{3d} spectra of cerium-bearing catalysts," *Chemical Engineering Journal* 170(1), 342-343. DOI: 10.1016/j.cej.2011.01.085

Pereao, O., Laatikainen, K., Bode-Aluko, C., Kochnev, L., Fatoba, O., Nechaev, A. N., and Petrik, L. (2019). "Adsorption of Ce^{3+} and Nd^{3+} by diglycolic acid functionalised electrospun polystyrene nanofiber from aqueous solution," *Separation and Purification Technology* 233, article ID 116059. DOI: 10.1016/j.seppur.2019.116059

Reindl, A. R., Saniewska, D., Grajewska, A., Falkowska, L., and Saniewski, M. (2021). "Alimentary exposure and elimination routes of rare earth elements (REE) in marine mammals from the Baltic Sea and Antarctic coast," *Science of the Total Environment* 754, article ID 141947. DOI: 10.1016/j.scitotenv.2020.141947

Saleh, T. A., Sarı, A., and Tuzen, M. (2017). "Effective adsorption of antimony(III) from aqueous solutions by polyamide-graphene composite as a novel adsorbent," *Chemical Engineering Journal* 307, 230-238. DOI: 10.1016/j.cej.2016.08.070

Sayyed, A. J., Deshmukh, N. A., and Pinjari, D. V. (2019). "A critical review of manufacturing processes used in regenerated cellulosic fibres: Viscose, cellulose acetate, cuprammonium, LiCl/DMAc, ionic liquids, and NMMO based lyocell," *Cellulose* 26, 2913-2940. DOI: 10.1007/s10570-019-02318-y

Sert, Ş., Kütahyali, C., İnan, S., Talip, Z., Çetinkaya, B., and Eral, M. (2008). "Biosorption of lanthanum and cerium from aqueous solutions by *Platanus orientalis* leaf powder," *Hydrometallurgy* 90(1), 13-18. DOI: 10.1016/j.hydromet.2007.09.006

Singh, P., Hegde, M. S., and Gopalakrishnan, J. (2008). "$Ce_{2/3}Cr_{1/3}O_{2+y}$: A new oxygen storage material based on the fluorite structure," *Chemistry of Materials* 40(23), 7268-7273. DOI: 10.1021/cm802207a

Sitko, R., Turek, E., Zawisza, B., Malicka, E., Talik, E., Heimann, J., Gagor, A., Feist, B., and Wrzalik, R. (2013). "Adsorption of divalent metal ions from aqueous solutions using graphene oxide," *Dalton Transactions* 42(16), 5682-5689. DOI: 10.1039/c3dt33097d

Song, J., Wang, X., and Chang, C. T. (2014). "Preparation and characterization of graphene oxide," *Journal of Nanomaterials* 2014, 1-6. DOI: 10.1155/2014/276143

Sverdrup, L. E., Källqvist, T., Kelley, A. E., Fürst, C. S., and Hagen, S. B. (2001). "Comparative toxicity of acrylic acid to marine and freshwater microalgae and the significance for environmental effects assessments," *Chemosphere* 45(4), 653-658. DOI: 10.1016/S0045-6535(01)00044-3

Torab-Mostaedi, M., Asadollahzadeh, M., Hemmati, A., and Khosravi, A. (2015). "Biosorption of lanthanum and cerium from aqueous solutions by grapefruit peel: equilibrium, kinetic and thermodynamic studies," *Research on Chemical Intermediates* 41(2), 559-573. DOI: 10.1007/s11164-013-1210-4

Wang, S., Lu, A., and Zhang, L. (2016). "Recent advances in regenerated cellulose materials," *Progress in Polymer Science* 53, 169-206. DOI: 10.1016/j.progpolymsci.2015.07.003

Wang, W., Li, Y., Li, W., Zhang, B., and Liu, Y. (2019a). "Effect of solvent pre-treatment on the structures and dissolution of microcrystalline cellulose in lithium chloride/dimethylacetamide," *Cellulose* 26, 3095-3109. DOI: 10.1007/s10570-019-02300-8

Wang, Y., Wang, D., Yi, N., Sheng, P., and Yang, B. (2019b). "Relationship between rare earth elements, lead and intelligence of children aged 6 to 16 years: A Bayesian structural equation modelling method," *International Archives of Nursing and Health Care* 5(2), article no. 123. DOI: 10.23937/2469-5823/1510123

Wang, N., Li, Y., Xie, L., Zhang, F., Ma, K., Chen, X., Hu, S., Yang, C., and Wang, X. (2020). "Cerium separation with $NaBiO_3$ nanoflower material via oxidation adsorption strategy," *Journal of Materials Chemistry A* 8(16), 7907-7913. DOI: 10.1039/d0ta01852j

Yuan, F. Y., Zhang, H. B., Li, X., Ma, H. L., Li, X. Z., and Yu, Z. Z. (2014). "*In situ* chemical reduction and functionalization of graphene oxide for electrically conductive phenol formaldehyde composites," *Carbon* 68, 653-661. DOI: 10.1016/j.carbon.2013.11.046

Zhang, X., Yu, H., Yang, H., Wan, Y., Hu, H., Zhai, Z., and Qin, J. (2015). "Graphene oxide caged in cellulose microbeads for removal of malachite green dye from aqueous solution," *Journal of Colloid and Interface Science* 437, 277-282. DOI: 10.1016/j.jcis.2014.09.048

Zhong, X., Liang, W., Lu, Z., Qiu, M., and Hu, B. (2020). "Ultra-high capacity of graphene oxide conjugated covalent organic framework nanohybrid for U(VI) and Eu(III) adsorption removal," *Journal of Molecular Liquids* 323, article ID 114603. DOI: 10.1016/j.molliq.2020.114603

Zhu, Y., Wang, W., Zheng, Y., Wang, F., and Wang, A. (2016). "Rapid enrichment of rare-earth metals by carboxymethyl cellulose-based open-cellular hydrogel adsorbent from HIPEs template," *Carbohydrate Polymers* 140, 51-58. DOI: 10.1016/j.carbpol.2015.12.003

Article submitted: March 4, 2022; Peer review completed: May 14, 2022; Revised version received and accepted: June 29, 2022; Published: July 7, 2022.
DOI: 10.15376/biores.17.3.4905-4920